

Ezrin Controls the Macromolecular Complexes Formed between an Adapter Protein Na⁺/H⁺ Exchanger Regulatory Factor and the Cystic Fibrosis Transmembrane Conductance Regulator*

Received for publication, March 1, 2005, and in revised form, August 26, 2005. Published, JBC Papers in Press, August 28, 2005, DOI 10.1074/jbc.M502305200

Jianquan Li, Zhongping Dai, Deirdre Jana, David J. E. Callaway, and Zimei Bu¹

From the Fox Chase Cancer Center, Philadelphia, Pennsylvania 19111

Na⁺/H⁺ exchanger regulatory factor (NHERF) is an adapter protein that is responsible for organizing a number of cell receptors and channels. NHERF contains two amino-terminal PDZ (postsynaptic density 95/disk-large/zonula occluden-1) domains that bind to the cytoplasmic domains of a number of membrane channels or receptors. The carboxyl terminus of NHERF interacts with the FERM domain (a domain shared by protein 4.1, ezrin, radixin, and moesin) of a family of actin-binding proteins, ezrin-radixin-moesin. NHERF was shown previously to be capable of enhancing the channel activities of cystic fibrosis transmembrane conductance regulator (CFTR). Here we show that binding of the FERM domain of ezrin to NHERF regulates the cooperative binding of NHERF to bring two cytoplasmic tails of CFTR into spatial proximity to each other. We find that ezrin binding activates the second PDZ domain of NHERF to interact with the cytoplasmic tails of CFTR (C-CFTR), so as to form a specific 2:1:1 (C-CFTR)₂·NHERF·ezrin ternary complex. Without ezrin binding, the cytoplasmic tail of CFTR only interacts strongly with the first amino-terminal PDZ domain to form a 1:1 C-CFTR·NHERF complex. Immunoprecipitation and immunoblotting confirm the specific interactions of NHERF with the full-length CFTR and with ezrin *in vivo*. Because of the concentrated distribution of ezrin and NHERF in the apical membrane regions of epithelial cells and the diverse binding partners for the NHERF PDZ domains, the regulation of NHERF by ezrin may be employed as a general mechanism to assemble channels and receptors in the membrane cytoskeleton.

Na⁺/H⁺ exchanger regulator factor (NHERF)² is an adaptor protein that is responsible for organizing membrane channels and receptors (1,

2). NHERF was originally identified as an essential cofactor for inhibiting a transmembrane transporter sodium-hydrogen exchanger isoform 3 (NHE3) by the cAMP-dependent protein kinase A in the kidney proximal tubule cells (1). However, subsequent studies find that NHERF is densely distributed in the apical membranes of polarized epithelial cells of several mammalian tissues (2, 3) and that NHERF participates in organizing the trafficking, localization, and membrane targeting of a large number of membrane receptors and channels to which NHERF binds (3–12).

NHERF is a multidomain and multivalent protein that recruits different signaling partners. The amino terminus of NHERF contains two modular PDZ (name derived from the first three proteins that this domain was identified postsynaptic density 95/disk-large/zonula occluden-1) domains, PDZ1 and PDZ2 (see Fig. 1). The NHERF PDZ domains bind to the consensus PDZ-binding motif D(S/T)X(V/I/L) (X denoting any amino acid residue) at the carboxyl termini of a number of membrane channels or receptors (13–19). The carboxyl terminus of NHERF recognizes the FERM domain (a conserved domain that is shared by protein 4.1, ezrin, radixin, and moesin) of a family of cytoskeletal actin-binding proteins, ezrin-radixin-moesin, which are collectively denoted as ERM proteins (Fig. 1). Thus, NHERF is also responsible for bridging the interactions between cell membrane and the cytoskeletal actin networks.

As a membrane cytoskeleton adapter protein, NHERF enhances the efficiency and specificity of membrane processes by forming multiprotein macromolecular complexes (20). For example, recent compelling evidence demonstrates that the macromolecular complexes recruited by NHERF can form homo- and hetero-oligomers between cystic fibrosis transmembrane conductance regulator (CFTR) and other membrane proteins to facilitate the efficient function of CFTR (21, 22, 21–25). CFTR is the most dominant Cl⁻ channel in several epithelial tissues, where it is responsible for salt and fluid transport (26). The CFTR Cl⁻ channel is cAMP-dependent protein kinase- and ATP-regulated. Impaired transport activities by CFTR are related to the genetic disease of cystic fibrosis (27). The PDZ domains of NHERF interact with the PDZ-binding motif DTRL at the carboxyl terminus of CFTR (3, 13, 28). Electrophysiological studies from Foskett's group show that the interactions of NHERF with CFTR can stimulate CFTR channel activities (24). Another study from the same group finds that phosphorylation of Ser-162 in the PDZ2 domain of NHERF by protein kinase C disrupts the binding between PDZ2 and CFTR and abolishes the ability of NHERF to stimulate CFTR gating (29). Based on these studies, Raghuram *et al.* (29) have proposed that when both PDZ domains of NHERF bind to two cytoplasmic tails of CFTR, the formed complex brings two CFTR monomers together and increases the open probability of CFTR channels. These studies together with the finding that

* This work was supported by the National Institutes of Health Grant CA06927, American Cancer Society Grant IRG-92-027-09, and by an appropriation from the commonwealth of Pennsylvania. The costs of publication of this article were defrayed in part by the payment of page charges. This article must therefore be hereby marked "advertisement" in accordance with 18 U.S.C. Section 1734 solely to indicate this fact.

¹ To whom correspondence should be addressed: Fox Chase Cancer Center, Reimann 414, 333 Cottman Ave., Philadelphia, PA 19111. Tel.: 215-728-7051; Fax: 215-728-3574; E-mail: Zimei.Bu@fccc.edu.

² The abbreviations used are: NHERF, Na⁺/H⁺ exchanger regulatory factor; CFTR, cystic fibrosis transmembrane conductance regulator; C-CFTR, the last 70 amino acid residues (1411–1480) at the carboxyl terminus of CFTR; ERM, ezrin-radixin-moesin; FERM, a conserved domain of ~300 amino acid residues shared by a family proteins that include protein 4.1, ezrin, radixin, and moesin; ezFERM, the FERM domain of ezrin; NHE3, Na⁺/H⁺ exchanger isoform 3; PDZ, a modular domain whose name is derived from the first three proteins (postsynaptic density 95, disk-large, zo-1) from which this domain is discovered; PDZ1, the first amino-terminal PDZ domain of NHERF, amino acid residues 11–99; PDZ2, the second PDZ domains of NHERF, amino acid residues 150–240; PDZ1-PDZ22, fragment of NHERF containing the PDZ1 and PDZ2 domains, residues 11–240; PDZ2-CT, truncated NHERF containing the PDZ2 domain and the C terminus, residues 150–358; RU, response unit in surface plasmon resonance experiments; SPR, surface plasmon resonance; SAXS, small angle x-ray scattering; TBS, Tris-buffered saline.

another four PDZ-containing CFTR-associated protein of 70 kDa (CAP70) interacts with the carboxyl-terminal tails of CFTR to generate a more active CFTR channel (23), demonstrating that multi-PDZ-domain adapter proteins promote the association of CFTR and stimulate CFTR channel activities.

In addition to promoting CFTR-CFTR interactions, NHERF also organizes the interaction between β_2 -adrenergic receptor and CFTR (25). By recruiting both CFTR and β_2 -adrenergic receptor, NHERF can physically cross-link β_2 -adrenergic receptor and CFTR into a single signaling complex. Consequently, β_2 -adrenergic receptor exercises its regulation on CFTR activities through NHERF (21, 22).

The ERM proteins to which NHERF binds are also important linkers between cell membranes and the cytoskeletal networks (30–32). The ERM proteins are localized in the apical actin-rich regions of polarized epithelial cells. They contribute to the functional organizations of specialized cell membrane domains in which many transmembrane channels and receptor reside and are localized. The association of NHERF with sodium-hydrogen exchanger isoform 3 (NHE3) and ezrin is also shown to be essential for cAMP-mediated phosphorylation and inhibition of NHE3 (33). The conformation and activity of the ERM proteins are considered to be negatively regulated by intramolecular interactions (34). In the inactive state of ezrin, the amino-terminal FERM domain of ezrin of ~300 amino acid residues is proposed to bind to the carboxyl terminus of ezrin with high affinity through a head-to-tail autoregulatory mechanism (35). After ezrin is activated by phosphorylation and/or phospholipid binding, the FERM domain releases the carboxyl terminus of ezrin. The activated FERM domain binds to NHERF, whereas the carboxyl-terminal domain of ezrin interacts with the actin filaments of the cytoskeleton network (36–38).

The above cell biological and physiological studies demonstrate the important physiological roles of NHERF in organizing membrane channels and receptors. It has also been proposed that the interaction of NHERF with membrane channels and transporters and with ezrin promotes the anchoring of these membrane proteins to the actin cytoskeleton to maintain their functions (33, 39). However, how NHERF interacts with ezrin to regulate the assembly of membrane proteins is not known. Here we report a combination of biophysical and *in vivo* studies to show that ezrin regulates the cooperative assembly of CFTR cytoplasmic domains by NHERF. Due to the high distributions of NHERF and ezrin in the apical membranes of polarized epithelial cells, the ezrin-regulated cooperative formation of NHERF recruited macromolecular complexes may be employed as a general mechanism to control the assembly and function of membrane channels and receptors by the membrane cytoskeleton.

MATERIALS AND METHODS

Protein Expression and Purification—The cDNAs encoding the full-length human NHERF-1 and ezrin were purchased from American Type Culture Collection (ATCC, Manassas, VA). The cDNA encoding the human CFTR was kindly provided by Dr. J. Kevin Foskett (University of Pennsylvania). We have employed the pET 100/D-TOPO and pET 151/D-TOPO expression systems (Invitrogen) to express proteins in *Escherichia coli*. Both the pET100/D-TOPO and the pET151/D-TOPO encode amino-terminal 6 \times His tags. The pET151/D-TOPO vector also encodes a V5-epitope tag at the amino terminus of the expressed proteins, whereas the pET100/D-TOPO vector expresses an amino-terminal Xpress-epitope tag in the expressed proteins.

The cDNA regions encoding the amino acid sequences of 11–99 (PDZ1), 150–240 (PDZ2), 11–240 (PDZ1-PDZ2), 150–358 (PDZ2-CT), 11–358 of NHERF, the FERM domain of ezrin 1–298 of ezrin

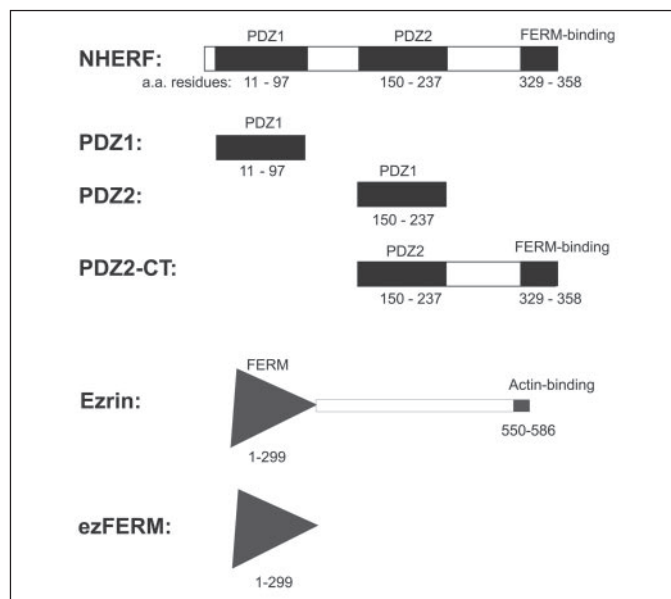


FIGURE 1. An illustration of the PDZ domains of NHERF along the primary sequence. The carboxyl terminus of NHERF, called the FERM-binding domain, recognizes a family of cytoskeleton actin binding ERM proteins. The amino-terminal FERM domain and the carboxyl terminus of ezrin are also shown.

(ezFERM), and the last 70 amino acid residues (1411–1480) at the carboxyl terminus of CFTR (C-CFTR) were amplified by PCR, respectively. The PCR products were inserted in the expression vectors. After transformation of the plasmids in BL21(DE3) cells, the cells were grown on large scale, harvested by centrifugation, and re-suspended with 30 ml of suspension buffer per liter of culture containing 20 mM sodium phosphate buffer (pH 7.5), 150 mM NaCl, 0.1 mM phenylmethylsulfonyl fluoride, and 10 mM imidazole.

The proteins were first purified by a HiTrap chelating column (Amersham Biosciences) pre-charged with Co^{2+} and pre-equilibrated with the binding buffer (20 mM phosphate, 0.1 mM phenylmethylsulfonyl fluoride, 10 mM imidazole, and 0.5 M NaCl, pH 7.5). The proteins were then further purified and analyzed by gel filtration chromatography using an ÄKTA fast-protein liquid chromatograph (Amersham Biosciences) with a Superdex 200 10/30 column (Amersham Biosciences). The molecular masses of the expressed proteins, calculated according to their amino acid sequences, were 14.0 kDa for PDZ1, 14.2 kDa for PDZ2, 27.0 kDa for PDZ2-CT, 29.4 kDa for PDZ1-PDZ2, 42.3 kDa for NHERF, 39.2 kDa for ezFERM, and 12.5 kDa for C-CFTR. The protein concentrations were determined by UV absorbance at 276 nm using the extinction coefficients calculated by the website ExPASy Proteomics Server (us.expasy.org/).

Solution Light Scattering Experiments—Light scattering experiments were performed on a DynaPro Molecular Sizing Instrument with Dynamics V6 data analysis software (Protein Solutions, Inc.). This instrument has the capability of conducting both static light scattering and dynamic light scattering experiments simultaneously. Static light scattering determines the absolute molecular weight of the protein or protein complex in solution, whereas dynamic light scattering measures the hydrodynamic radius R_h and estimates the monodispersity of the protein samples. Before light scattering experiments, the samples were centrifuged at 10,000 rpm for 5 min to remove dust. About 24 μl of protein solution was then loaded to the DynaPro cell. At least 60 acquisitions (10 s/acquisition) were collected for each sample. The average of these acquisitions is reported. Light scattering experiments were conducted at 25 $^{\circ}\text{C}$.

Ezrin Modulates NHERF to Bring Two CFTRs into Proximity

Surface Plasmon Resonance—Surface plasmon resonance (SPR) experiments were carried out on BIAcore 1000 instrument. The hydrogel matrix of a BIAcore CM5 Biosensor chip was activated by *N*-hydroxysuccinimide and *N*-ethyl-*N'*-[3-(diethylamino)propyl]carbodiimide. For studying the binding between C-CFTR and the differently truncated forms of NHERF (or the NHERF·ezFERM complex), the sensor chip was coated with C-CFTR by injecting 3 μ l of C-CFTR at 5 μ g/ml in 10 mM sodium acetate, pH 5.2, over the activated SPR sensor chip. For studying the binding of ezFERM to NHERF (or ezFERM binding to the C-CFTR·NHERF complex), the sensor chip was coated with ezFERM by injecting 3 μ l of 10 μ g/ml ezFERM in 10 mM sodium acetate, pH 5.2, over the activated surface. Uncross-linked ligand was washed away, and uncoated sites were blocked by 1 M ethanolamine, pH 8.5. The ligand density was controlled by the maximum binding response signal ranging from 150 to 200 response units (RUs). The analytes, NHERF, PDZ2-CT, PDZ2-CT·ezFERM, NHERF·ezFERM, at a series of concentrations were injected over the C-CFTR-coated surface at 50 μ l/min for 3 min, respectively. The analytes, NHERF or C-CFTR·NHERF complex, were injected over the ezFERM-coated sensor chip.

The response curves were obtained by subtracting the background signal, generated from a control cell injected with the same analyte but without ligand coating of the hydrogel matrix to remove the bulk refractive index effects. The nonspecific binding was corrected by subtracting the signal generated from buffer alone. The binding curve reached an equilibrium plateau in all cases. The RU value corresponding to the plateau was taken as a measure to obtain the binding curves. The binding curves were fit to either the monovalent binding model to obtain K_d or to the bivalent binding model to obtain K_{d1} or K_{d2} (40).

Cell Culture and Delivering Proteins in Mammalian Cells—BHK cells were kindly provided by Dr. Gergely L. Lukacs (the Hospital for Sick Children, Toronto). The BHK cells were maintained in Dulbecco's modified Eagle's medium supplemented with 10% fetal calf serum at 37 °C in a humidified 5% CO₂ atmosphere. The cells were grown in a 6-well plate with wells of 30-mm diameter.

The BioTrek Protein Delivery Regent (Stratagene) was used to deliver NHERF or the NHERF·ezFERM complex in BHK cells. Purified NHERF and the NHERF·ezFERM complex were diluted to 150 μ g/ml using phosphate-buffered saline buffer. The purified NHERF has an amino-terminal V5-epitope tag, and the purified ezFERM has an amino-terminal Xpress-epitope tag. About 100 μ l of the diluted protein solution was transferred to the tube containing the lyophilized BioTrek reagent. The lyophilized reagent was resuspended by pipetting the protein solution up and down for 3–5 times. The BioTrek-protein mixtures were then left at room temperature for ~5 min. Serum-free medium was then added to the tube to a final volume of 500 μ l.

When the cell density reached 50–60% confluence, the culture medium was removed from the wells by aspiration. The cells were washed once with serum-free medium. After 500 μ l of fresh serum-free medium was added to each well, 500 μ l of the BioTrek-protein mixture was added dropwise to the cells. The cell culture plate was then incubated at 37 °C and 5% CO₂ in a humidified incubator for 4–5 h before immunoprecipitation experiments. When delivering both NHERF and ezFERM in BHK cells, we first delivered ezFERM in cells 2 h before delivering NHERF in cells. The cells were then incubated for 2 h after NHERF was delivered.

Immunoprecipitation and Immunoblotting Experiments—Cell monolayers in 30-mm-diameter wells were washed with phosphate-buffered saline buffer followed by lysis in radioimmune precipitation assay buffer at 4 °C. About 10 μ g of mouse anti-V5 antibody (Invitro-

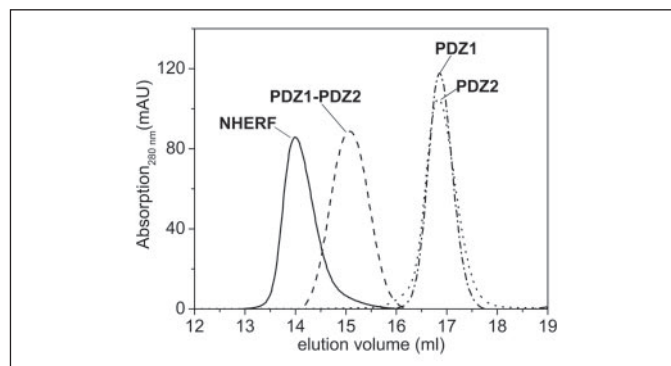


FIGURE 2. Gel filtration characterization of different truncated constructs of NHERF. Light scattering analysis of NHERF solution shows that NHERF is a monomer when the protein concentration is below 1.3 mg/ml (see TABLE ONE).

gen) was added to 500 μ g of cell lysate, and the mixture was shaken in a cold room for 4 h to pull-down NHERF. Protein G PLUS-agarose beads (Santa Cruz Biotechnology) of 20 μ l were added, and the mixture was shaken in a cold room overnight. The beads were then spun and washed three times with 750 μ l of radioimmune precipitation assay buffer and re-suspended in 50 μ l of SDS-PAGE sample buffer. In another experiment, ~10 μ g of mouse anti-Xpress antibody (Invitrogen) was added to 500 μ g of cell lysate to pull-down ezFERM.

After electrophoresis, proteins in the SDS-PAGE gel were transferred to nitrocellulose membranes by semi-dry blotting. The membranes were then blocked in 5% fat-free milk in TBS-T (10 mM Tris-HCl, pH 7.5, 150 mM NaCl, 0.05% Tween-20) for 3 h at room temperature. The primary rabbit anti-CFTR antibody (Alomone Laboratory) was used for detecting CFTR, mouse anti-V5 antibody for NHERF detection, or mouse anti-Xpress antibody for ezFERM detection. The primary antibody was added to the blots and incubated overnight in blocking solution. The following day the blots were washed with TBS-T buffer for three times and then incubated with the secondary antibody (anti-mouse-horseradish peroxidase for mouse anti-V5 and anti-Xpress primary antibodies, or anti-rabbit-horseradish peroxidase for rabbit anti-CFTR primary antibody) for 1 h at room temperature and washed for three times with changes of TBS-T buffer. The blots were then developed by enhanced chemiluminescent detection ECL (Pierce) for analysis.

Solution Small Angle X-ray Scattering—The SAXS experiments were performed with an in-house apparatus (Rigaku/Osmic, Inc.) with a Q range from 0.009 to 0.30 \AA^{-1} , where $Q = 4\pi \sin(\theta/2)/\lambda$ is the magnitude of the scattering vector, θ is the scattering angle, and λ is the wavelength of the x-ray. Data treatments have been described previously (41, 42).

The reduced scattering data are plotted as scattering intensity $I(Q)$ versus Q profiles. The radius of gyration R_g , which is related to the size and shape of a protein, can be obtained from the Guinier approximation (43, 44), $\ln I(Q) = \ln I(0) - (1/3)Q^2 R_g^2$, by linear least squares fitting in the $QR_g < 1$ region. The forward scattering intensity $I(0)$ is linearly proportional to the molecular weight of the protein complexes. Inverse Fourier transformation of $I(Q)$ gives the length distribution function $P(r)$, which is the probability of finding two scattering points at a given distance r from each other in the measured macromolecule. $P(r)$ functions were generated by the program GNOM (45). The value at which $P(r)$ becomes 0 reflects the maximum molecular dimension D_{\max} of the macromolecule averaged over all orientations. The shape of $P(r)$ function and the value of D_{\max} can be used to deduce the macromolecular shape and the distance between two domains within the protein. The program DAMMIN (46) was used to reconstruct the low resolution

TABLE ONE

Summary of molecular masses and size information about NHERF and the complexes by light scattering experiments

Species and stoichiometry ^a in complex	Molecular mass by SLS	Calculated molecular mass	R _h by DLS ^b
	kDa		Å
NHERF at 1.3 mg/ml	45.3 ± 0.3	42.3	46.0 ± 0.5
NHERF/ezFERM (1:1) at 1.0 mg/ml	81.2 ± 0.2	81.5	52.0 ± 0.4
C-CFTR/NHERF (1:1) at 1.3 mg/ml	55.1 ± 0.4	54.8	51.3 ± 0.6
PDZ2-CT/ezFERM (1:1) at 1.8 mg/ml	67.5 ± 0.3	66.2	47.4 ± 0.4
C-CFTR/PDZ2-CT/ezFERM (1:1:1) at 1.6 mg/ml	78.8 ± 0.4	78.7	52.0 ± 0.5
(C-CFTR) ₂ /NHERF/ezFERM (2:1:1) at 2.7 mg/ml	108.3 ± 0.4	106.5	63.0 ± 0.5
C-CFTR/NHERF/ezFERM (1:1:1) at 1.0 mg/ml	94.8 ± 0.7 (at 11.3ml) ^c	94.0	58.2 ± 0.6
	94.4 ± 0.3 (at 11.9ml) ^c		

^a The stoichiometry of the complexes was obtained from the molecular weights measured by SLS.

^b The hydrodynamic radius obtained from DLS.

^c The fractions were taken from fractions P1 and P2 during gel filtration as shown in Fig. 6

three-dimensional molecular structures from SAXS data. The program Situs (47) was used to dock the fragments of known crystal structures (PDZ1 and ezFERM) to the low resolution structures. More details about the procedures for reconstruction of the three-dimensional molecular images from solution SAXS data have been described previously (48).

RESULTS

The Cytoplasmic Tail of CFTR and NHERF Form a Discrete Complex with 1:1 Stoichiometry

As an adapter protein, NHERF organizes the assembly of protein complexes. It is of interest to know the oligomer states and the global conformation of the intact NHERF to understand how NHERF provides a scaffold for protein binding partners in complexes. Our gel filtration and light scattering experiments show that the oligomeric states of NHERF are concentration-dependent. At protein concentrations of above 5 mg/ml, the oligomerization of NHERF is apparent (data not shown). However, when the protein concentration is lowered to below 1.3 mg/ml, both gel filtration and light scattering experiments show that NHERF exists as a monomer with a measured molecular mass of 45.3 kDa (Fig. 2 and TABLE ONE). As we show in the following studies, it is the monomeric state of NHERF that is responsible for interacting with the cytoplasmic tail of CFTR and the FERM domain of ezrin. NHERF monomer is thus the functional form in this study. The NHERF dimeric and higher oligomeric states probably play an inhibitory role to prevent NHERF from binding to other partners.

The stoichiometry and binding affinity of C-CFTR to the intact NHERF were determined by a combination of gel filtration, solution static light scattering, dynamic light scattering, and SPR experiments. After 25.0 μM NHERF was incubated with C-CFTR at different molar ratios overnight, the formed complex was separated by gel filtration (Fig. 3). The gel filtration chromatograms with the incubation molar ratios of C-CFTR to NHERF at 1:1 and 2:1 are shown in Fig. 3. All molar ratios of incubation produce only one new peak, which is eluted at ~12.9 ml. Light scattering experiments show that the eluted complexes do not aggregate and have a molecular mass of 55.1 kDa (see TABLE ONE), which suggests the formation of a 1:1 C-CFTR·NHERF complex.

SPR experiments were conducted to determine the affinity and stoichiometry of NHERF to C-CFTR binding. Fig. 4A shows the C-CFTR to NHERF binding curve obtained from SPR experiments, which can be best fitted by the bivalent equilibrium binding model (40) with two quite different dissociation constants, $K_{d1} = 288$ nM and $K_{d2} = 1098$ nM. We then performed a series of SPR experiments to compare the C-CFTR binding properties of individual PDZ domains. These different truncations are PDZ1, PDZ2, the two tandem PDZ1-PDZ2, and PDZ2-CT

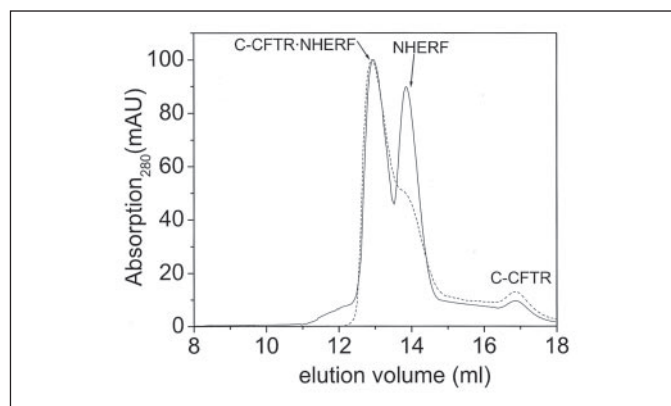


FIGURE 3. C-CFTR and NHERF form a complex with 1:1 stoichiometry. Using gel filtration to identify the formation of the C-CFTR-NHERF complex. The solid line is the equimolar incubation of C-CFTR-NHERF, and the dashed line is the 2:1 incubation. Light scattering experiments on the gel filtration eluted C-CFTR-NHERF complex (at 1.3 mg/ml) gives a molecular mass of 55.1 kDa, indicating a 1:1 stoichiometry of binding.

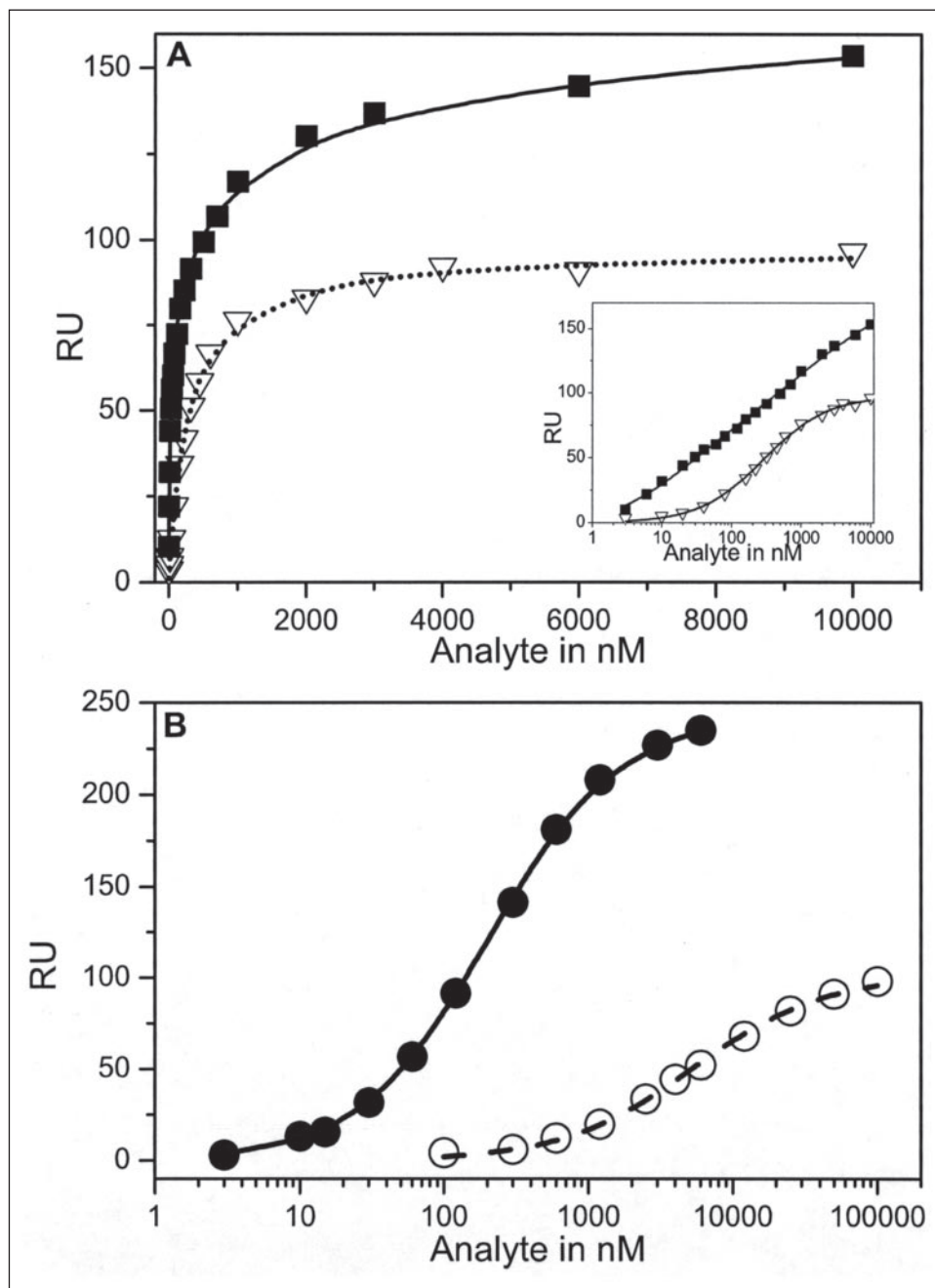
(with the PDZ1 domain removed from NHERF). The obtained dissociation constants are summarized in TABLE TWO. The binding affinity of PDZ1 for C-CFTR ($K_d = 298$ nM) is over 16-fold stronger than that of PDZ2 ($K_d = 4800$ nM). PDZ2 and PDZ2-CT have similar binding affinities for C-CFTR ($K_d = 4800$ nM for PDZ2, and $K_d = 5300$ nM for PDZ2-CT). PDZ1-PDZ2 has a bivalent binding behavior similar to that of NHERF.

Comparing the dissociation constants of C-CFTR·NHERF binding with those of the variously truncated NHERF constructs, we are able to assign the bivalent C-CFTR·NHERF dissociation constant K_{d1} as C-CFTR/PDZ1 binding, which is strong, and K_{d2} as C-CFTR/PDZ2 binding, which is weak (see TABLE TWO). TABLE TWO also shows that the PDZ1 domain in the construct of PDZ1-PDZ2 and in the full-length NHERF do not show any changes in binding affinity for C-CFTR when compared with that of the individual PDZ1 domain, suggesting that the binding affinity of PDZ1 to C-CFTR is high and remains changed by truncations.

The FERM Domain of Ezrin and NHERF Form a Tight Binary Complex with 1:1 Stoichiometry

Previous studies have identified the interaction between NHERF and the FERM domain of ezrin (ezFERM) (49). We have examined the affinity and the stoichiometry of NHERF binding to ezFERM by gel filtration, light scattering, and SPR experiments. After 10.0 μM

FIGURE 4. Equilibrium SPR analysis of C-CFTR binding to NHERF and to the NHERF-ezFERM complex. The binding of ezFERM at the carboxyl terminus of NHERF activates PDZ2 to have an increased binding affinity for C-CFTR and thus change the stoichiometry of interaction of NHERF with C-CFTR. *A*, the binding of NHERF (∇) to C-CFTR as a function of NHERF concentrations, and the binding of NHERF-ezFERM (\blacksquare) to C-CFTR as a function of NHERF-ezFERM concentrations (labeled as analyte). The lines are fits to the bivalent model (40). *Inset* is same data set with the analyte concentrations plotted on logarithmic scales in order to show the difference in binding affinities. The *inset* shows that NHERF-ezFERM has higher overall binding affinities for C-CFTR than NHERF does. The lines are fits to the bivalent model. *B*, the binding of C-CFTR to PDZ2-CT (O) as a function of PDZ2-CT concentrations, and the binding of C-CFTR to PDZ2-CT-ezFERM (\bullet) as a function of PDZ2-CT-ezFERM concentrations.



ezFERM was incubated with different molar ratios of NHERF overnight, the formed complexes were eluted at a retention volume of ~ 12.6 ml in the gel filtration chromatogram. Fig. 5A shows the formation of the complex of NHERF with ezFERM by a gel filtration experiment.

Light scattering experiments on the eluted complex show that the NHERF-ezFERM complex does not form aggregates and has a discrete hydrodynamic radius of $R_h = 54 \text{ \AA}$ (TABLE ONE). The molecular mass of the complex, measured by light scattering is 81.2 kDa (TABLE ONE), suggesting that NHERF and ezFERM form a 1:1 complex. The stoichiometry of the NHERF-ezFERM complex was further verified by the monovalent binding behavior in SPR experiments with a dissociation constant of $K_d = 19 \text{ nM}$ (see Fig. 5B). These experiments show a strong and specific 1:1 binding between NHERF and ezFERM.

Binding of ezFERM to NHERF Activates the PDZ2 Domain and Changes the Stoichiometry of NHERF to C-CFTR Binding

Two Types of 1:1:1 Ternary Complex Formed between C-CFTR and NHERF-ezFERM—After C-CFTR was incubated with the binary NHERF-ezFERM complex at equimolar ratio, the complex could be identified and separated by gel filtration (Fig. 6A). At equimolar ratio of incubation of C-CFTR with NHERF-ezFERM, two peaks P1 and P2 are observed on the gel filtration chromatogram at retention volumes of 11.3 and 11.9 ml, respectively. Light scattering experiments show that the molecular masses of these two fractions are the same, to be 94.8 and 94.4 kDa, respectively (see TABLE ONE). The gel filtration and light scattering results thus suggest that the two kinds of ternary complexes have the same binding stoichiometry of 1:1:1, presented as C-CFTR·NHERF·ezFERM.

TABLE TWO

Summary of the binding constants measured by SPR

The K_d values are obtained from the plots of the response unit of equilibrium plateau against the analyte concentrations by fitting into either monovalent or bivalent model. K_{d1} was assigned to the binding affinity of the PDZ1 domain of NHERF, and K_{d2} to that of PDZ2, respectively.

Monovalent analyte	K_d	
	nM	
PDZ1	298 ± 10	
PDZ2	4800 ± 300	
PDZ2-CT	5300 ± 200	
PDZ2-CT/ezFERM	202 ± 3	
Bivalent analyte	K_{d1}	K_{d2}
	nM	
PDZ1-PDZ2	283 ± 42	1247 ± 120
NHERF	288 ± 32	1098 ± 96
NHERF/ezFERM	204 ± 39	16 ± 2

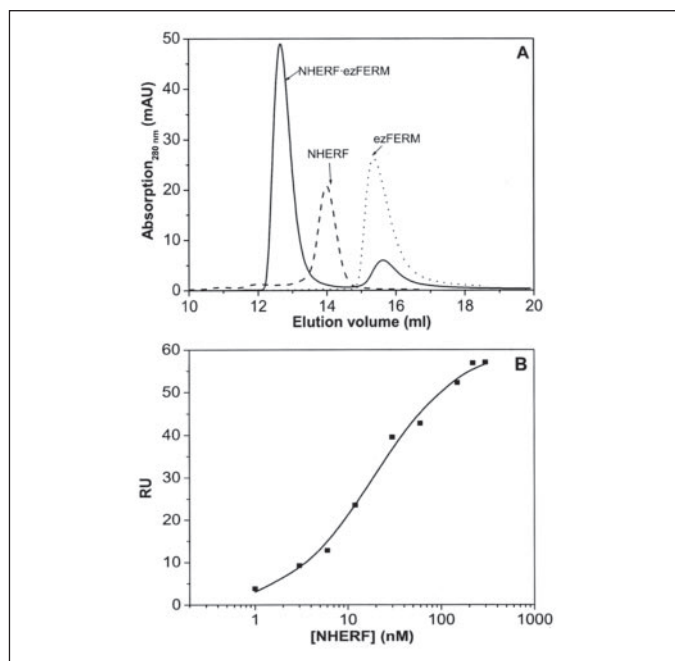


FIGURE 5. NHERF and ezFERM form a complex with 1:1 stoichiometry. *A*, gel filtration chromatography shows the complex formed when equimolar NHERF and ezFERM are incubated. Light scattering shows that the molecular weight of the complex is 81.2 kDa (see TABLE ONE), indicating the formation of a 1:1 hetero-dimer. *B*, equilibrium SPR analysis of NHERF-efFERM binding. The line is a fit to the monovalent binding model with $K_d = 19$ nM.

The different elution volumes of the two peaks during gel filtration reflect a significant difference in sizes and molecular shapes of these two 1:1:1 complexes. The fraction eluted at 11.3 ml is a ternary complex with C-CFTR bound to the first PDZ domain of the binary NHERF-efFERM complex, whereas that elutes at 11.9 ml is the one with C-CFTR binding to the second PDZ domain. This is because the binding of C-CFTR at the PDZ1 domain of NHERF-efFERM binary complex can cause the ternary complex to be more elongated, and thus to have a larger size than the other ternary complex with C-CFTR binding to the middle PDZ2 domain. However, the hydrodynamic radii of the two peak fractions measured by dynamic light scattering are similar with $R_h = 58.2$ and 58.1 Å, respectively (TABLE ONE), suggesting a rapid re-equilibration of the two complexes during dynamic light scattering measurements. In summary, these experiments suggest that the PDZ2 domain of NHERF in the NHERF-efFERM complex has an increased binding affini-

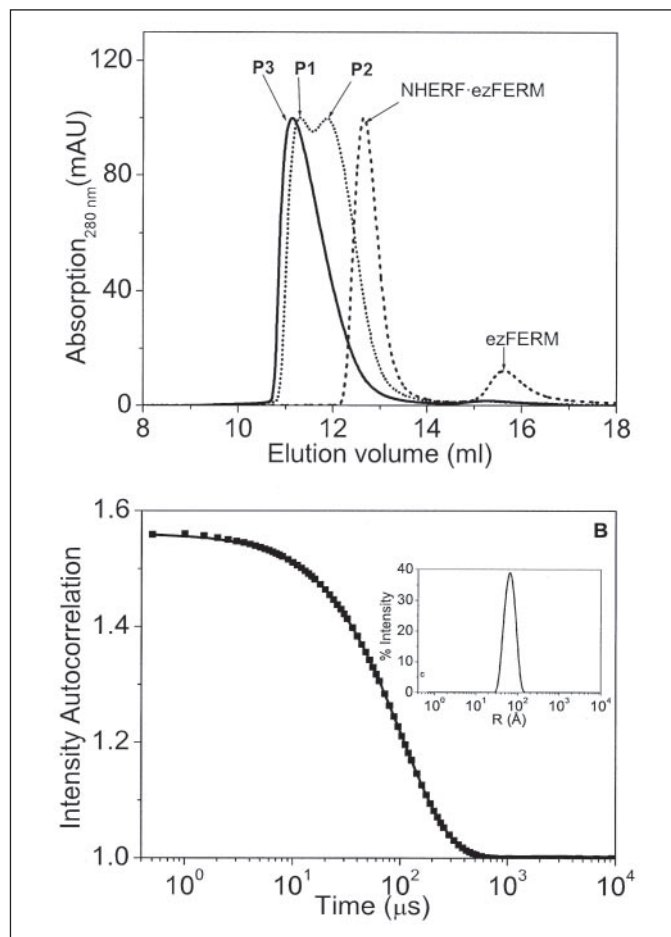


FIGURE 6. Binding of ezFERM to NHERF changes the stoichiometry of NHERF binding to C-CFTR. *A*, gel filtration analysis of the different C-CFTR-NHERF-efFERM complexes. *B*, dynamic light scattering on the (C-CFTR)₂-NHERF-efFERM ternary complex at 2.7 mg/ml. Because only one intensity distribution peak is observed, the measured protein and protein complexes are monodispersed. The scattered intensity normalized by protein concentration gives a molecular mass of 108.3 kDa, suggesting the formation of a ternary complex with 2:1:1 stoichiometry.

ity to the cytoplasmic tails of CFTR, as compared with that in the intact NHERF alone.

Formation of the 2:1:1 (C-CFTR)₂-NHERF-efFERM Ternary Complex—We then incubated C-CFTR with the NHERF-efFERM complex at 2:1 molar ratio. Gel filtration chromatogram of this incubation shows a single peak P3 (see Fig. 6A). The elution volume of this peak fraction at 11.1 ml suggests that a complex is formed during gel filtration, which is larger than both the 1:1:1 C-CFTR-NHERF-efFERM complexes. Light scattering analysis of this peak fraction shows that this ternary complex does not aggregate, with a hydrodynamic radius being $R_h = 65$ Å, suggesting the formation of a discrete complex (see Fig. 6B and TABLE ONE). The molecular mass measured by light scattering is 108.3 kDa (TABLE ONE), indicating a 2:1:1 binding stoichiometry and the formation of (C-CFTR)₂-NHERF-efFERM ternary complex.

The SPR analysis suggests that the C-CFTR to NHERF-efFERM binding curve is best fitted with the bivalent equilibrium binding model with two dissociation constants $K_{d1} = 204$ nM and $K_{d2} = 16$ nM (see Fig. 4A and TABLE TWO). Fig. 4A shows that the binding affinity of C-CFTR for the NHERF-efFERM binary complex is significantly different from that of C-CFTR to NHERF binding, in terms of both the magnitude of the SPR RU signals and the positions of the mid points of the binding curves. First, the K_{d2} of C-CFTR to NHERF-efFERM binding has decreased by nearly 69-fold when compared with the K_{d2} (TABLE

Ezrin Modulates NHERF to Bring Two CFTRs into Proximity

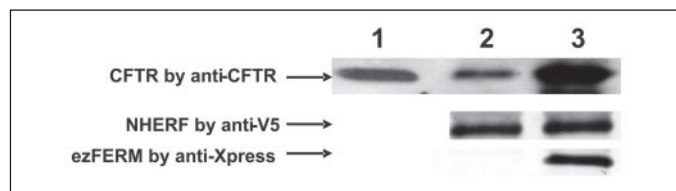


FIGURE 7. Immunoprecipitation and immunoblotting to determine the interaction of NHERF with CFTR and with ezFERM in mammalian cells. Lane 1 is the immunoblot of the full-length CFTR from the BHK cell lysate. Lane 2 is the immunoblot of CFTR and NHERF of the immunoprecipitation complex from BHK cells after NHERF is delivered in cells. Lane 3 is the immunoblot of CFTR, NHERF, and ezFERM of the immunoprecipitation complex from BHK cells after both ezFERM and NHERF are delivered in the BHK cells.

TWO) of C-CFTR to NHERF binding. Secondly, the RU signal of the C-CFTR and NHERF·ezFERM interaction is nearly twice that of C-CFTR to NHERF binding when the two binding events reach their respective saturation points. Thus the SPR analysis shows that, as a result of binding ezFERM to NHERF, NHERF changes its stoichiometry of interaction with C-CFTR, with the formation of a 2:1:1 (C-CFTR)₂·NHERF·ezFERM complex *versus* a 1:1 C-CFTR·NHERF complex.

Next, we identify which PDZ domain of NHERF has an increased binding affinity for C-CFTR when the FERM domain of ezrin is bound to the NHERF carboxyl terminus. We have compared the binding behaviors of C-CFTR to differently truncated constructs of NHERF. TABLE TWO shows that the K_d of PDZ1 to C-CFTR binding is similar to K_{d1} of PDZ1-PDZ2 to C-CFTR binding. The K_d of PDZ1 is also similar to the K_{d1} of NHERF and that of NHERF·ezFERM complex. Thus, comparing the K_d values of PDZ1 in different truncation constructs and in different complex forms suggests that the PDZ1 domain of NHERF has an intrinsically high binding affinity for C-CFTR, and that its binding affinity is not affected by ezrin binding to NHERF, or by the presence of the PDZ2 domain of NHERF.

To examine how PDZ2 changes its C-CFTR binding properties, we have analyzed the binding properties of a truncated construct PDZ2-CT, with the second PDZ domain and the carboxyl terminus intact. Without binding of ezFERM at the carboxyl terminus of PDZ2-CT, the affinity of PDZ2-CT for C-CFTR is weak with a $K_d = 5300$ nM (see TABLE TWO and Fig. 4B). The binding affinity of PDZ2-CT for C-CFTR is as weak as that of the individual PDZ2 domain for C-CFTR. However, when the carboxyl terminus of PDZ2-CT is bound to ezFERM, the affinity C-CFTR for PDZ2-CT·ezFERM is significantly increased with a $K_d = 202$ nM (see Fig. 4B and TABLE TWO). Light scattering experiments shows that PDZ2-CT·ezFERM can form a discrete 1:1 complex (see TABLE ONE). The SPR and light scattering experiments suggest that it is the PDZ2 domain of NHERF that has an increased binding affinity to C-CFTR when the FERM domain of ezrin is bound to the carboxyl terminus of NHERF.

Thus, the results show that binding of the FERM domain of ezrin at the NHERF carboxyl terminus change the stoichiometry of C-CFTR to NHERF interaction. We also demonstrate that it is the PDZ2 domain of NHERF that has an increased binding affinity for C-CFTR, whereas the binding affinity of PDZ1 remains unchanged by ezrin binding.

Immunoprecipitation and Immunoblotting Show the Specific Interactions of NHERF with Full-length CFTR and with the FERM Domain of Ezrin *in Vivo*—We have conducted immunoprecipitation and immunoblotting experiments to determine the interactions of NHERF with ezFERM and with the full-length CFTR in BHK cells. BHK cells generated by Lukacs' group can constitutively express full-length CFTR (50, 51). In Fig. 7, lane 1 shows the immunoblotting of CFTR from the BHK cell lysate.

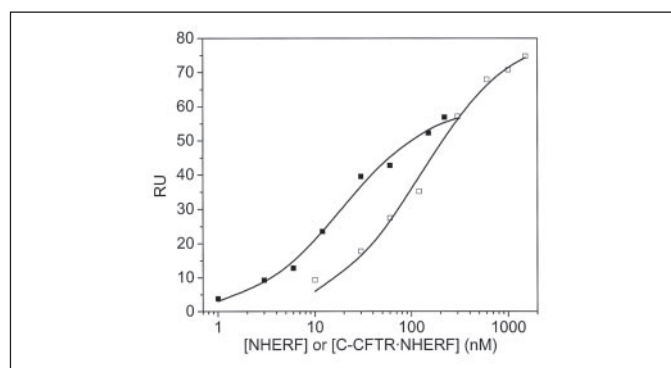


FIGURE 8. SPR analysis of the decreased binding affinity of ezFERM for NHERF when C-CFTR is bound to NHERF. The solid square is the binding of NHERF to ezFERM. The open square is the binding of C-CFTR·NHERF to ezFERM. The lines are fittings to the monovalent binding model.

We first determined the interaction of NHERF with CFTR in BHK cells. After the purified NHERF (with an amino-terminal V5 epitope tag) was delivered in BHK cells for 4–5 h, the cells were lysed. Anti-V5 antibody was used to pull down NHERF in immunoprecipitation. Immunoblotting shows that the immunoprecipitated complex contains both the full-length CFTR and NHERF (see lane 2 of Fig. 7).

The purified ezFERM and NHERF were then delivered separately in BHK cells to determine the interactions of NHERF with CFTR and with ezFERM in cells. The purified ezFERM contains an amino-terminal Xpress-epitope tag. Anti-V5 was used to pull-down the NHERF during immunoprecipitation. Immunoblotting shows that the immunoprecipitated complex contains CFTR, NHERF, and ezFERM, see lane 3 of Fig. 7. Similar results to that shown in Fig. 7 are obtained by using anti-Xpress antibody to pull down ezFERM during immunoprecipitation. Thus, the immunoprecipitation and immunoblotting results show that NHERF specifically interacts with the full-length CFTR and with the FERM domain of ezrin to form a ternary complex *in vivo*.

The amount of the immunoprecipitated complex that we have loaded in lanes 2 and 3 of Fig. 7 are the same during SDS-PAGE electrophoresis. A comparison of the band intensities of CFTR bands in lanes 2 and 3 suggests that the NHERF·ezFERM complex can bind more CFTR in BHK cells. Thus, Fig. 7 shows that *in vivo* study also indicates that NHERF·ezFERM has an increase binding affinity to CFTR. However, we believe that the biophysical methods we reported in this study are more rigorous to determine the binding affinity and stoichiometry of the complexes than immunoprecipitation experiments (52).

Binding of C-CFTR to the First PDZ Domain of NHERF Decreases the Binding Affinity of the Carboxyl Terminus of NHERF to the FERM Domain of Ezrin—SPR was used to analyze the binding of the FERM domain of ezrin to the C-CFTR·NHERF complex. After incubation of equimolar C-CFTR and NHERF, the binary complex was separated by gel filtration. The C-CFTR·NHERF binary complex at various concentrations was injected over an ezFERM domain-coated SPR sensor chip. The results, shown in Fig. 8, suggest that the binding between the FERM domain of ezrin and the binary complex C-CFTR·NHERF is monovalent with a dissociation constant $K_d = 125$ nM (also listed in TABLE TWO), which is over 6-fold higher than that of ezFERM to NHERF binding ($K_d = 19$ nM) without the presence of C-CFTR. The NHERF in the C-CFTR·NHERF complex thus has an obviously lower binding affinity for ezFERM than NHERF alone.

The Three-dimensional Architecture of the (C-CFTR)₂·NHERF·ezFERM Ternary Complex—We then determined the low resolution structure of

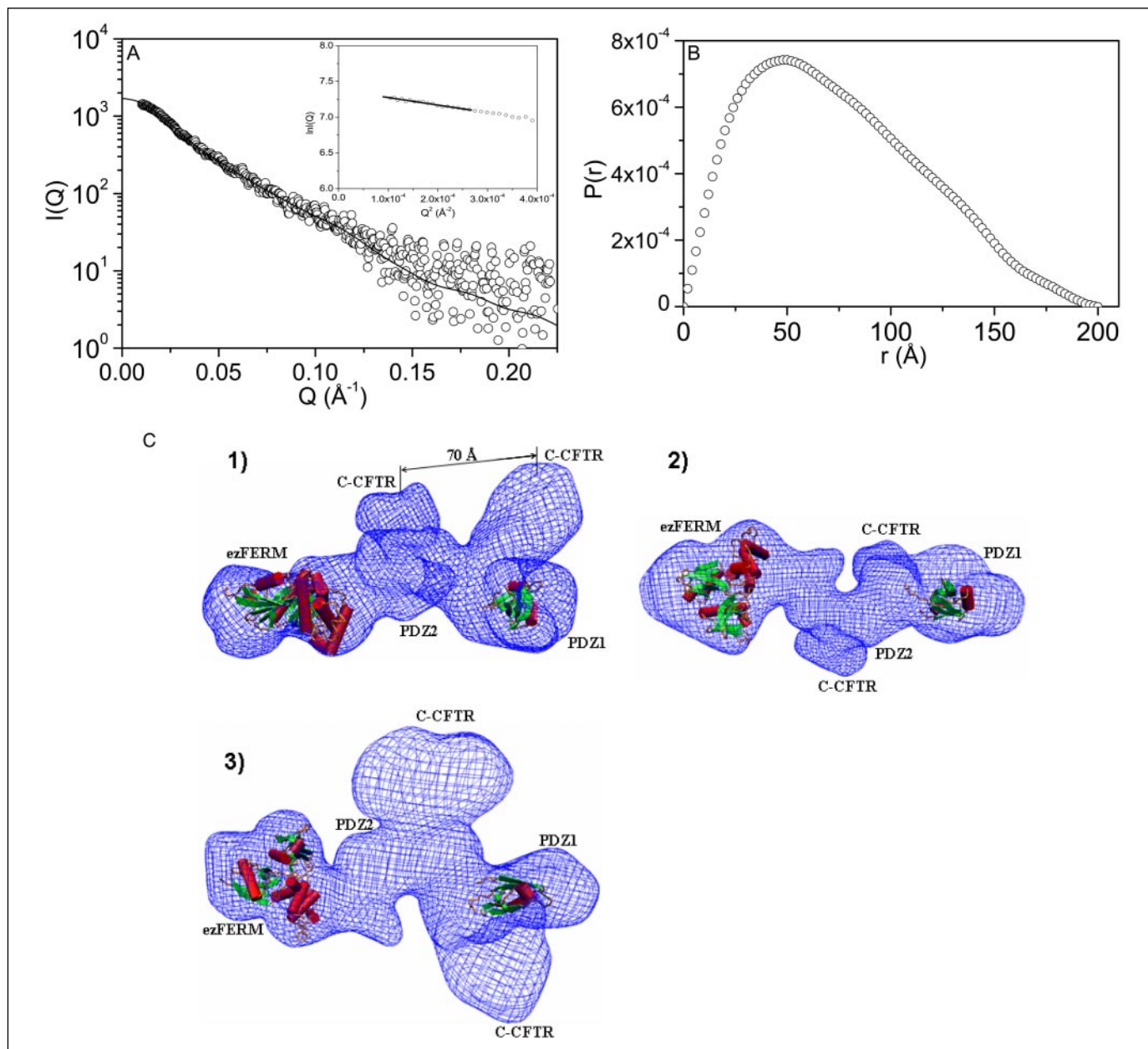


FIGURE 9. Solution SAXS analysis of the C-CFTR-NHERF-ezFERM ternary complex. *A*, scattering profile of the ternary complex (C-CFTR)₂·NHERF·ezFERM at 1.6 mg/ml. The lines are *ab initio* fits with $\chi^2 = 1.5$. The inset is the Guinier plot data. The lines are the linear fittings to the Guinier plots (in the $QR_g \leq 1$ region) to obtain the radii of gyration. *B*, $P(r)$ functions of the (C-CFTR)₂·NHERF·ezFERM ternary complex. *C*, the molecular envelope of the (CFTR)₂·NHERF·ezFERM ternary complex reconstructed from SAXS. 1, side view; 2, a looking-down view; 3, a looking-up view, opposite to that shown in 2. The available crystal structures of the FERM domain of ezrin (Protein Data Bank Code: 1NI2.pdb) and the PDZ1 domain of NHERF (Protein Data Bank Code: 1G9O.pdb) are docked to the reconstructed envelope. The graphics are generated using VMD (65).

the 2:1:1 (C-CFTR)₂·NHERF·ezFERM ternary complex by SAXS. The SAXS-measured complex has a radius of gyration $R_g = 62.2 \text{ \AA}$ (Fig. 9*A*, inset). The complex adopts an elongated conformation with the maximum dimension $D_{\max} = 200 \text{ \AA}$ for the 2:1:1 complex (see Fig. 9*B*). The overall three-dimensional molecular envelope of the ternary complex reconstructed from SAXS is shown in Fig. 9*C*. In Fig. 9*C*, we can identify the two lobes representing the two C-CFTR molecules being anchored to the PDZ1 and PDZ2 domains of NHERF. At the other end of the envelope of the ternary complex, the triangular shape representing ezFERM can be identified. Fig. 9*C* shows that the distance between the two C-CFTR lobes is $\sim 70 \text{ \AA}$ (shown in Fig. 9*C*), a value that is close to the reported diameter of $\sim 66 \text{ \AA}$ of a CFTR dimer channel from a freeze-fracture electron microscopy study (53).

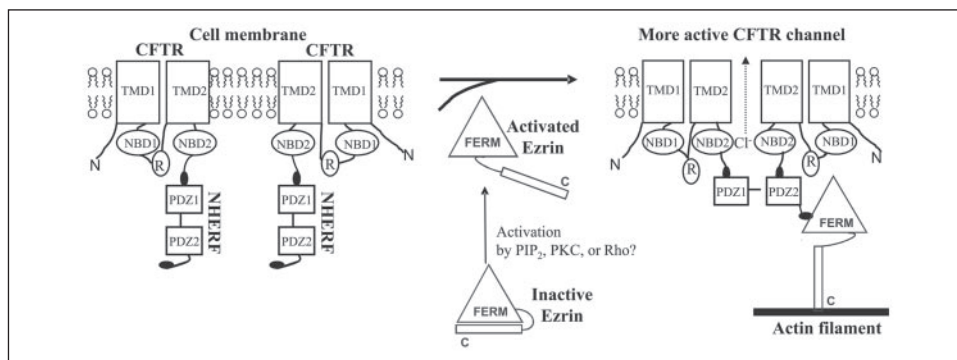
DISCUSSION

In this study, we have demonstrated that binding of the FERM domain of ezrin at the carboxyl terminus of NHERF significantly increases the binding affinity of the NHERF PDZ2 domain for the carboxyl terminus of CFTR. Our results thus suggest that ezrin can positively regulate the cooperative binding of NHERF to C-CFTR. As a result of ezrin binding, a specific ternary complex (C-CFTR)₂·NHERF·ezFERM of 2:1:1 stoichiometry is formed, in which two C-CFTR molecules are anchored to NHERF. The immunoprecipitation and immunoblotting experiments demonstrate the specific interactions of NHERF with the full-length CFTR and with ezrin *in vivo*.

An organized actin cytoskeleton network is believed to be required

Ezrin Modulates NHERF to Bring Two CFTRs into Proximity

FIGURE 10. A model to show the regulation of NHERF by ezrin which changes the stoichiometry of NHERF to CFTR binding. TMD, transmembrane domain; NBD, the nucleotide-binding domain; R, the regulatory domain. After ezrin binds to the carboxyl terminus of NHERF, the PDZ2 domain is activated to bind to C-CFTR. As a result, NHERF brings two CFTR cytoplasmic tails into proximity to each other. The schematic also shows that the carboxyl terminus of ezrin binds to the filamentous actin.



for the cAMP-dependent activation of CFTR channels (54). The specific (CFTR)₂·NHERF·ezrin interaction provides a pathway to transmit signals from the cytoskeleton actin network to regulate CFTR activities. Ezrin is a cytoskeleton actin linker protein. When the intact ezrin is in the inactive state, the amino-terminal FERM domain self-associates with the last 30 amino acid residues of ezrin carboxyl terminus (34). Ezrin is considered to be activated upon phosphorylation at Tyr-145, Tyr-353, and/or Thr-567 (55–57) and by phospholipid binding (31). The activated ezrin releases its own carboxyl terminus from the FERM domain. The exposed FERM domain can then bind to the carboxyl terminus of NHERF (37), whereas the carboxyl terminus of an activated ezrin can bind to actin filaments (31). Thus, we propose a model of sequential protein-protein interaction events, consisting of initial ezrin activation (Fig. 10), followed by ezrin to NHERF binding. The subsequent activation of PDZ2 enables NHERF to bring two CFTR carboxyl termini into proximity to each other, and as a result, to generate a more active CFTR channel. Consequently, the regulatory signals can be transmitted from the cytoskeletal actin network. Other members in ERM family might also adopt this mechanism to interact with NHERF in transmitting the regulatory signal from the cytoskeletal network to regulate transmembrane proteins.

In Fig. 8, we have also shown that the presence of C-CFTR in the PDZ1 domain of NHERF reduces the affinity of the NHERF carboxyl terminus for ezFERM by ~6-fold. The reduction in binding affinity suggests that binding of C-CFTR to the PDZ1 domain of NHERF can negatively regulate the interaction of NHERF with ezFERM. The negative cooperativity implies that the (CFTR)₂·NHERF·ezFERM assembly may not play a significant role in transmitting signal from CFTR to the actin cytoskeletal network. Rather, the transmission of signal is unidirectional. That is, the signal is transmitted from the actin cytoskeletal network to ezrin and then to the CFTR channel. Alternatively, this weakened NHERF-ezrin interaction, due to the binding of CFTR to the PDZ1 domain of NHERF, can also serve as a feedback loop to weaken the interaction of the PDZ2 domain with CFTR, by uncoupling ezrin binding to NHERF. As a result, the stimulation of CFTR channel due to the activation of NHERF by ezrin is weakened. Nevertheless, the overall 2:1:1 complex (C-CFTR)₂·NHERF·ezFERM is stable, which may indicate that the binding of C-CFTR to the PDZ2 domain of NHERF stabilizes the interaction between the NHERF carboxyl terminus and ezrin.

Our findings have broad implications, because the ezrin-modulated NHERF binding stoichiometry changes may also affect the specificity of NHERF binding to other NHERF target proteins that contain the PDZ domain binding motifs. For example, regulation of the activity of the transmembrane transporter Na⁺/H⁺ exchanger 3 (NHE3), of which NHERF is an essential cofactor, also requires ezrin and/or an intact cytoskeletal actin network for optimal function (33, 58). The target proteins may also include the platelet-derived growth factor receptor (8),

β₂-adrenergic receptor (3), CIC-3B channel (59), Na⁺/H⁺ exchanger 3 (NHE3) (60), PTH1 receptor (61), Yes-associated protein 65 (62), phospholipase C-β₃ (63), and NHERF phosphorylation kinase GRK6A (64). Ezrin may participate directly in regulating the activities of these target proteins by modulating the stoichiometry of their interactions with NHERF. The formation of these multiprotein complexes can influence the spatial arrangements of numerous receptors and channels.

To summarize, our results reveal that ezrin is a regulator that can positively control the cooperative binding of NHERF with the cytoplasmic domains of CFTR, thus modulating the stoichiometry of C-CFTR to NHERF interaction. In Fig. 10, we have proposed a model to show the assembly of a CFTR macromolecular complex that is regulated by NHERF whose binding stoichiometry to CFTR is in turn modulated by ezrin. This model is supported by our small angle x-ray scattering study of the three-dimensional architecture of the C-CFTR·NHERF·ezFERM ternary complex (see Fig. 9C). Due to the abundant distribution of NHERF and ezrin in polarized epithelial cells, the same mechanisms can be employed to regulate the activities of other membrane channels and receptors by the membrane cytoskeleton.

Acknowledgments—We thank G. L. Lukacs for kindly providing BHK cells, K. Foscett for kindly providing CFTR cDNA, and K. Campbell, G. D. Markharm, and H. Roder for comments on the manuscript.

REFERENCES

- Weinman, E. J., Steplock, D., Corry, D., and Shenolikar, S. (1993) *J. Clin. Invest.* **91**, 2097–2102
- Voltz, J. W., Weinman, E. J., and Shenolikar, S. (2001) *Oncogene* **20**, 6309–6314
- Hall, R. A., Ostedgaard, L. S., Premont, R. T., Blitzer, J. T., Rahman, N., Welsh, M. J., and Lefkowitz, R. J. (1998) *Proc. Natl. Acad. Sci. U. S. A.* **95**, 8496–8501
- Sneddon, W. B., Syme, C. A., Bisello, A., Magyar, C. E., Rochdi, M. D., Parent, J. L., Weinman, E. J., Abou-Samra, A. B., and Friedman, P. A. (2003) *J. Biol. Chem.* **278**, 43787–43796
- Li, J. G., Chen, C., and Liu-Chen, L. Y. (2002) *J. Biol. Chem.* **277**, 27545–27552
- Yoo, D., Flagg, T. P., Olsen, O., Raghuram, V., Foscett, J. K., and Welling, P. A. (2004) *J. Biol. Chem.* **279**, 6863–6873
- Brone, B., and Eggermont, J. (2005) *Am. J. Physiol.* **288**, C20–C29
- Maudsley, S., Zamah, A. M., Rahman, N., Blitzer, J. T., Luttrell, L. M., Lefkowitz, R. J., and Hall, R. A. (2000) *Mol. Cell. Biol.* **20**, 8352–8363
- Hall, R. A., Premont, R. T., Chow, C. W., Blitzer, J. T., Pitcher, J. A., Claing, A., Stoffel, R. H., Barak, L. S., Shenolikar, S., Weinman, E. J., Grinstein, S., and Lefkowitz, R. J. (1998) *Nature* **392**, 626–630
- Dai, J. L., Wang, L., Sahin, A. A., Broemeling, L. D., Schutte, M., and Pan, Y. (2004) *Oncogene* **23**, 8681–8687
- Hall, R. A., Spurney, R. F., Premont, R. T., Rahman, N., Blitzer, J. T., Pitcher, J. A., and Lefkowitz, R. J. (1999) *J. Biol. Chem.* **274**, 24328–24334
- Mahon, M. J., and Segre, G. V. (2004) *J. Biol. Chem.* **279**, 23550–23558
- Karthikeyan, S., Leung, T., and Ladas, J. A. (2001) *J. Biol. Chem.* **276**, 19683–19686
- Karthikeyan, S., Leung, T., Birrane, G., Webster, G., and Ladas, J. A. (2001) *J. Mol. Biol.* **308**, 963–973
- Karthikeyan, S., Leung, T., and Ladas, J. A. (2002) *J. Biol. Chem.* **277**, 18973–18978
- Ladas, J. A. (2003) *J. Membr. Biol.* **192**, 79–88

17. Songyang, Z., Fanning, A. S., Fu, C., Xu, J., Marfatia, S. M., Chishti, A. H., Crompton, A., Chan, A. C., Anderson, J. M., and Cantley, L. C. (1997) *Science* **275**, 73–77
18. Kornau, H. C., Schenker, L. T., Kennedy, M. B., and Seeburg, P. H. (1995) *Science* **269**, 1737–1740
19. Niethammer, M., Valtschanoff, J. G., Kapoor, T. M., Allison, D. W., Weinberg, T. M., Craig, A. M., and Sheng, M. (1998) *Neuron* **20**, 693–707
20. Shenolikar, S., Voltz, J. W., Cunningham, R., and Weinman, E. J. (2004) *Physiology (Bethesda)* **19**, 362–369
21. Guggino, W. B., and Banks-Schlegel, S. P. (2004) *Am. J. Respir. Crit. Care Med.* **170**, 815–820
22. Schwiebert, E. M., Benos, D. J., Egan, M. E., Stutts, M. J., and Guggino, W. B. (1999) *Physiol. Rev.* **79**, S145–S166
23. Wang, S., Yue, H., Derin, R. B., Guggino, W. B., and Li, M. (2000) *Cell* **103**, 169–179
24. Raghuram, V., Mak, D. D., and Foskett, J. K. (2001) *Proc. Natl. Acad. Sci. U. S. A.* **98**, 1300–1305
25. Naren, A. P., Cobb, B., Li, C., Roy, K., Nelson, D., Heda, G. D., Liao, J., Kirk, K. L., Sorscher, E. J., Hanrahan, J., and Clancy, J. P. (2003) *Proc. Natl. Acad. Sci. U. S. A.* **100**, 342–346
26. Sheppard, D. N., and Welsh, M. J. (1999) *Physiol. Rev.* **79**, S23–S45
27. Zielenski, J., and Tsui, L. C. (1995) *Annu. Rev. Genet.* **29**, 777–807
28. Wang, S., Raab, R. W., Schatz, P. J., Guggino, W. B., and Li, M. (1998) *FEBS Lett.* **427**, 103–108
29. Raghuram, V., Hormuth, H., and Foskett, J. K. (2003) *Proc. Natl. Acad. Sci. U. S. A.* **100**, 9620–9625
30. Reczek, D., and Bretscher, A. (1998) *J. Biol. Chem.* **273**, 18452–18458
31. Bretscher, A., Edwards, K., and Fehon, R. G. (2002) *Nat. Rev. Mol. Cell. Biol.* **3**, 586–599
32. Gautreau, A., Louvard, D., and Arpin, M. (2002) *Curr. Opin. Cell Biol.* **14**, 104–109
33. Weinman, E. J., Steplock, D., Donowitz, M., and Shenolikar, S. (2000) *Biochemistry* **39**, 6123–6129
34. Gary, R., and Bretscher, A. (1995) *Mol. Biol. Cell* **6**, 1061–1075
35. Pearson, M. A., Reczek, D., Bretscher, A., and Karplus, P. A. (2000) *Cell* **101**, 259–270
36. Algrain, M., Turunen, O., Vaheri, A., Louvard, D., and Arpin, M. (1993) *J. Cell Biol.* **120**, 129–139
37. Finnerty, C. M., Chambers, D., Ingraffea, J., Faber, H. R., Karplus, P. A., and Bretscher, A. (2004) *J. Cell Sci.* **117**, 1547–1552
38. Bretscher, A. (1999) *Curr. Opin. Cell Biol.* **11**, 109–116
39. Short, D. B., Trotter, K. W., Reczek, D., Kreda, S. M., Bretscher, A., Boucher, R. C., Stutts, M. J., and Milgram, S. L. (1998) *J. Biol. Chem.* **273**, 19797–19801
40. Herr, A. B., White, C. L., Milburn, C., Wu, C., and Bjorkman, P. J. (2003) *J. Mol. Biol.* **327**, 645–657
41. Bu, Z., and Engelman, D. M. (1999) *Biophys. J.* **77**, 1064–1073
42. Bu, Z., Perlo, A., Johnson, G. E., Olack, G., Engelman, D. M., and Wyckoff, H. W. (1998) *J. Appl. Crystallogr.* **31**, 533–543
43. Glatter, O., and Kratky, O. (1982) *Small Angle X-ray Scattering*, pp. 15–17, Academic Press, New York
44. van Holde, K. E., Johnson, W. C., and Ho, P. S. (1998) *Principles of Physical Biochemistry*, p. 325, Prentice Hall, Upper Saddle River, NJ
45. Semenyuk, A. V., and Svergun, D. I. (1991) *J. Appl. Crystallogr.* **24**, 537–540
46. Svergun, D. I. (1999) *Biophys. J.* **76**, 2879–2886
47. Wriggers, W., and Chacón, P. (2001) *J. Appl. Crystallogr.* **34**, 773–776
48. Ho, D. L., Byrnes, W. M., Ma, W. P., Shi, Y., Callaway, D. J., and Bu, Z. (2004) *J. Biol. Chem.* **279**, 39146–39154
49. Reczek, D., and Bretscher, A. (2001) *J. Cell Biol.* **153**, 191–206
50. Haardt, M., Benharouga, M., Lechardeur, D., Kartner, N., and Lukacs, G. L. (1999) *J. Biol. Chem.* **274**, 21873–21877
51. Benharouga, M., Sharma, M., So, J., Haardt, M., Drzymala, L., Popov, M., Schwapach, B., Grinstein, S., Du, K., and Lukacs, G. L. (2003) *J. Biol. Chem.* **278**, 22079–22089
52. Masters, S. C. (2004) *Methods Mol. Biol.* **261**, 337–350
53. Eskandari, S., Wright, E. M., Kreman, M., Starace, D. M., and Zampighi, G. A. (1998) *Proc. Natl. Acad. Sci. U. S. A.* **95**, 11235–11240
54. Prat, A. G., Cunningham, C. C., Jackson, G. R., Jr., Borkan, S. C., Wang, Y., Ausiello, D. A., and Cantiello, H. F. (1999) *Am. J. Physiol.* **277**, C1160–C1169
55. Krieg, J., and Hunter, T. (1992) *J. Biol. Chem.* **267**, 19258–19265
56. Pietromonaco, S. F., Simons, P. C., Altman, A., and Elias, L. (1998) *J. Biol. Chem.* **273**, 7594–7603
57. Matsui, T., Maeda, M., Doi, Y., Yonemura, S., Amano, M., Kaibuchi, K., and Tsukita, S. (1998) *J. Cell Biol.* **140**, 647–657
58. Weinman, E. J., Steplock, D., Wade, J. B., and Shenolikar, S. (2001) *Am. J. Physiol. Renal. Physiol.* **281**, F374–F380
59. Ogura, T., Furukawa, T., Toyozaki, T., Yamada, K., Zheng, Y. J., Katayama, Y., Nakaya, H., and Inagaki, N. (2002) *FASEB J.* **16**, 863–865
60. Yun, C. H., Oh, S., Zizak, M., Steplock, D., Tsao, S., Tse, C. M., Weinman, E. J., and Donowitz, M. (1997) *Proc. Natl. Acad. Sci. U. S. A.* **94**, 3010–3015
61. Mahon, M. J., Donowitz, M., Yun, C. C., and Segre, G. V. (2002) *Nature* **417**, 858–861
62. Mohler, P. J., Kreda, S. M., Boucher, R. C., Sudol, M., Stutts, M. J., and Milgram, S. L. (1999) *J. Cell Biol.* **147**, 879–890
63. Hwang, J. I., Heo, K., Shin, K. J., Kim, E., Yun, C., Ryu, S. H., Shin, H. S., and Suh, P. G. (2000) *J. Biol. Chem.* **275**, 16632–16637
64. Hall, R. A., Premont, R. T., and Lefkowitz, R. J. (1999) *J. Cell Biol.* **145**, 927–932
65. Humphrey, W., Dalke, A., and Schulten, K. (1996) *J. Molec. Graphics* **14**, 33–38